Published online 9 December 2022 *Nucleic Acids Research, 2022, Vol. 50, No. 22* **12723–12738**
https://doi.org/10.1093/nar/gkac1063

TEAD1 regulates cell proliferation through a pocket-independent transcription repression mechanism

Feng Li[1,*], Vinny Negi[1], Ping Yang[1], Jeongkyung Lee[1], Ke Ma[2], Mousumi Moulik[3] and Vijay K. Yechoor[1,*]

[1]Division of Endocrinology, Diabetes and Metabolism, Department of Medicine, University of Pittsburgh, Pittsburgh, PA, USA, [2]Department of Diabetes Complications and Metabolism, Diabetes and Metabolism Research Institute, City of Hope, Duarte, CA, USA and [3]Division of Pediatric Cardiology, Department of Pediatrics, University of Pittsburgh, Pittsburgh, PA, USA

Received August 25, 2022; Revised October 13, 2022; Editorial Decision October 21, 2022; Accepted November 28, 2022

ABSTRACT

The Hippo-TEAD pathway regulates cellular proliferation and function. The existing paradigm is that TEAD co-activators, YAP and TAZ, and co-repressor, VGLL4, bind to the pocket region of TEAD1 to enable transcriptional activation or repressive function. Here we demonstrate a pocket-independent transcription repression mechanism whereby TEAD1 controls cell proliferation in both non-malignant mature differentiated cells and in malignant cell models. TEAD1 overexpression can repress tumor cell proliferation in distinct cancer cell lines. In pancreatic β cells, conditional knockout of TEAD1 led to a cell-autonomous increase in proliferation. Genome-wide analysis of TEAD1 functional targets via transcriptomic profiling and cistromic analysis revealed distinct modes of target genes, with one class of targets directly repressed by TEAD1. We further demonstrate that TEAD1 controls target gene transcription in a motif-dependent and orientation-independent manner. Mechanistically, we show that TEAD1 has a pocket region-independent, direct repressive function via interfering with RNA polymerase II (POLII) binding to target promoters. Our study reveals that TEAD1 target genes constitute a mutually restricted regulatory loop to control cell proliferation and uncovers a novel direct repression mechanism involved in its transcriptional control that could be leveraged in future studies to modulate cell proliferation in tumors and potentially enhance the proliferation of normal mature cells.

INTRODUCTION

The Hippo pathway is an evolutionarily-conserved mechanism from Drosophila to mammals in tissue development and growth processes by modulating cell proliferation, differentiation, and death (1). Yes-associated protein (YAP) and WW domain-containing transcription regulator protein 1 (WWTR1, TAZ) are critical effector components in the Hippo signaling cascade. YAP and TAZ, as co-regulators, do not have DNA binding domains and associate with TEAD transcription factors (TEA domain) to modulate transcription for target gene regulation (2–3). Thus, TEAD factors link upstream and downstream signals in the Hippo pathway. In mammals, there are four genes encoding homologous members of the TEAD family, TEAD1–4, which recognize the MCAT sequence motif (GGAATG) on its gene targets (4). In addition to YAP and TAZ co-activators for TEADs, VGLL4 was reported to be a TEAD co-repressor (5). Interestingly, YAP and TAZ could also function as TEAD co-repressors to suppress DDIT4 (DNA-damage-inducible transcript 4) and Trail (TNF-related apoptosis-inducing ligand) transcription (6). To date, cofactors are considered to be necessary for TEAD to control target genes involved in the regulation of cell growth and cell proliferation. Crystallography analyses revealed that TEAD N-terminus binds with MCAT elements while its C-terminus is responsible for interaction with cofactors (7–8). Structural analysis indicates that a pocket area within TEAD is the interface that mediates cofactor binding, formed by β4, β11, β12, α1 and α4 of TEAD (7). The majority of available TEAD pathway inhibitors target this domain (8–11), although many molecules display poor potency (12). We hypothesized that an alternative regulatory mechanism may exist for TEAD modulation independent of its pocket structure, based on

*To whom correspondence should be addressed. Tel: +1 412 383 4251; Fax: +1 412 648 3290; Email: yechoorv@pitt.edu
Correspondence may also be addressed to Feng Li. Email: fenglimed@gmail.com

our recent finding that TEAD1 had transcriptional regulatory functions independent of YAP and TAZ (Feng Li *et al.* in press).

Many recent studies suggest the importance of TEAD in the development of human cancers. To date, in cancer research, most studies on TEAD activity are limited to serving as the functional readout of the Hippo-YAP/TAZ pathway. In hepatocellular carcinoma (HCC), dominant-negative TEAD reversed YAP-induced hepatomegaly and tumorigenesis *in vivo*. Moreover, VGLL4-mimicking peptide and verteporfin (a small YAP-binding chemical) were demonstrated to harbor therapeutic effects against YAP-induced tumorigenesis by interrupting TEAD-YAP interaction (8,13–14). However, YAP/TAZ-independent functions of TEAD factors in tumorigenesis remain elusive.

In contrast to its role in oncogenesis, TEAD1's function in mature differentiated cells is even less understood. Recent evidence highlights its role in the normal function of cardiomyocytes (15) and vascular smooth muscle (16). Pancreatic β-cell failure to compensate for the metabolic needs underlies all diabetes. While there is autoimmune-mediated β-cell destruction in Type 1 diabetes, in the late stages of type 2 diabetes, β-cell failure and reduction in functional β-cell mass lead to diabetes with hyperglycemia with consequent morbidity and mortality (17). Increasing β-cell functional mass through augmenting proliferation is a promising approach to ameliorating β-cell deficiency in diabetes. Pancreatic islets are post-mitotic unique mature cell types with dedicated insulin-secretion function and regulation, and many genes within the Hippo pathway, including YAP, are selectively repressed (18–19). In mature β cells, YAP expression is not detectable (20–21), suggesting repression of YAP could be involved in maintaining β-cell maturation. However, the mechanisms of YAP repression in adult β cells remain unknown. Among TEAD family members, TEAD1 is the most abundant in islets (22). Despite our current understanding of Hippo signaling, the roles of the TEAD pathway in regulating β cell proliferation remain unclear.

In the current study, to dissect the mechanisms underlying the potential role of TEAD1 in proliferation, we utilize three model systems with extremes of proliferation/differentiation function, with the pancreatic β cell being a highly differentiated cell type with low proliferative capacity, insulinoma-derived INS (INS1 and INS2) cells having a high proliferation with some retained function and HeLa cancer cell line with a high proliferative capacity. We demonstrate that conditional TEAD1 deletion in pancreatic β cells leads to an increase in proliferation with a loss of repression of a subset of target genes involved in enhancing proliferation, including YAP, while TEAD1 overexpression led to a repression of proliferation in both INS and HeLa cells with repression of a similar subset of target genes. Mechanistically we demonstrate that TEAD1 represses transcription in a pocket-independent manner for these genes, in part by preventing the binding of POLII to the TSS on the promoter. Taken together, we identify a transcriptional repressive mechanism of TEAD1 that is widely prevalent in cells that are normal, highly differentiated cells, and those that are malignant.

MATERIALS AND METHODS

Transgenic mouse generation and osmotic pumps implantation

All animal experiments were approved by the Institutional Animal Care and Use Committee of University of Pittsburgh. To generate pancreatic β-cell-specific TEAD1 knockout (TKO) transgenic line, TEAD1$^{flox/flox}$ mice (22) were bred with the mice carrying murine Ins1 promoter-driven Cre recombinase (#026801; The Jackson Laboratory). TEAD1 floxed alleles were confirmed using the genotyping PCR primers: forward (GCCTTCTGAGTGCTGGCATTAAAGG) and reverse (AAGGCAGACTCCTTCATTGGAATGG). Osmotic pumps (#1002; ALZET®) (delivery rate at 0.2 U/day for 14 days) that contain human insulin (Humulin® R REGULAR Insulin Human Injection U-100; Lilly) or vehicle (0.9% NaCl solution) were implanted subcutaneously in 4-week-old TKO or control mice (TEAD1$^{flox/flox}$/Cre^{-}). All the mice were housed under standard 12 h light–dark cycles with ad lib access to food and water unless otherwise specified.

In vivo tumorigenesis using J:NU nude mice

Upon reaching ∼80% confluence, TEAD1-overexpressed or vehicle lentiviral transduced HeLa cells were rinsed twice with phosphate buffered saline and detached from the culture dishes with 0.25% trypsin–EDTA solution (#25200056; Thermo Fisher Scientific). For *in vivo* tumorigenesis, 8×10^6 cells were resuspended in 100μl ice-cold culture medium (DMEM supplemented with 10% FBS; # 11965092; Thermo Fisher Scientific), which were injected subcutaneously into 5-week-old male J:NU nude mice (#007850; The Jackson Laboratory) ($n = 3$ each group) using 1ml syringes with 25G needles. Nodule formation was monitored by weekly palpations on the injection sites. Tumor size was assessed by external measurement of the length and width of the tumors in two dimensions using a caliper as soon as tumors reached measurable size. The tumor volume was calculated by the formula: volume $= 1/2 \times$ length (mm) $\times$ (width [mm])^2.

Bioinformatics analysis

TCGA database (https://genome-cancer.ucsc.edu/) (23) was employed to study the association between TEAD1 mRNA expression levels and any clinical outcomes. 33 cancer types were analyzed. All transcript counts were normalized to TPM or $\log_2$ converted when necessary. R (V3.6.3) was used for the statistical analysis. R package ggplot2 were used to analyze functional enrichment and visualize expression differences. The survival curve was constructed using the KM method and the log-rank test.

Plasmid construction and subcloning

Human NR4A3L, NR4A3S, VGLL4 and WTIP expression plasmids were purchased from Genescript (#OHu15070, #OMu68325, #OHu15880, and #OHu29047). Human

WWC2 cDNA ORF clone was purchased from Sino Biological Inc. (#HG19486-U). The Human PRKCI vector was a gift from Luke McCaffrey (#35387; Addgene). Human AMOTL2 vector was a gift from Tomasz Prószyński (#112833; Addgene). YAP5SA was a gift from Kunliang Guan (#27371; Addgene). Myc-tagged human TEAD1 vector was a gift from Kunliang Guan (#33109; Addgene). The CDS regions of human TEAD1, WWC2, PRKIC, AMOTL2, WTIP, YAP5SA, NR4A3L and NR4A3S were subcloned into the lentiviral backbone. The ΔTEAD1 vector was subcloned using the full-length TEAD1 vector as a template. All plasmids utilized in this study were validated by Sanger sequencing. Most of the lentiviral plasmids generated in this study will be deposited in Addgene (http://www.addgene.org/).

Modified split-GFP system

In the classical split-GFP system, the GFP is divided into three individual components, GFP1-9, GFP10 and GFP11. In the presence of GFP1–9, when proteins of interest fused to GFP10 and GFP11 interact, the assembly of the three parts of GFP enables fluorescence emission. We put GFP10 and GFP11 on both terminals of the bait and prey proteins, respectively, as an 'all-in-one' plasmid, including mCherry as a transfection tracking reporter to show the transfection efficiency. The backbone vector used for split-GFP system is pLenti-smURFP-T2A-mCherry (pLenti) (#80347; Addgene). The sequence for GFP10 is GGCA TGGATTTACCAGACGACCATTACCTGTCAACACA AACTATCCTTTCGAAAGATCTCAAC, and GFP11 is GAAAAGCGTGACCACATGGTCCTTCTTGAG TATGTAACTGCTGCTGGGATTACAGATGCTAGC. The sequences for 'GFP11-linker-Myc tag-*XbaI*:*SgsI*-linker-GFP11-T2A-GFP10-linker-*Pfl23II*:*SfaAI*-Flag tag-linker-GFP10' were synthesized by Integrated DNA Technologies (IDT). The fragment was inserted into pLenti via *BamHI*:*EcoRI* sites. The sequences for 'bait' proteins, including TEAD1 and ΔTEAD1, were inserted via *XbaI*:*SgsI* sites using In-Fusion® HD Cloning Kit (#638946; Takara Bio). The sequences for 'prey' proteins including YAP1, TAZ and VGLL4, were inserted via *Pfl23II*:*SfaAI* sites. The fragment EF1a-mCherry-P2A, subcloned from an Addgene plasmid (#135003), was ligated with GFP1-9 by overlapping PCR followed by insertion into pLenti via *XhoI*:*Acc65I* sites using In-Fusion® HD Cloning Kit. All plasmids utilized in this study were validated by Sanger sequencing.

Cell lines and plasmid transfections

Pancreatic β cell lines, INS1 and INS2, were cultured as previously described (22). HeLa and NT2 cell lines were purchased from ATCC (#CRM-CCL-2, #CRL-1973) and cultured following the recommended protocols by ATCC. For HEK293T cells, vector transfection was performed using the Lipofectamine 3000 kit (L3000015; Thermo Fisher) according to the manufacturer's instructions. For the INS1, INS2, HeLa and NT2 cells, vector transduction was performed with lentivirus.

Mouse islet isolation and culture

Mouse islets were isolated and purified as previously described (24). Briefly, 2–3 ml collagenase XI (1 mg/ml; #C7657; Sigma) dissolved in Hank's buffered saline solution (#55037C; Sigma) was injected into the mouse pancreas via the bile duct. The perfused pancreas was then incubated in collagenase buffer for 18 min at 37 °C and further dissociated by mechanical pipetting. Islets were hand-picked under a dissecting microscope. Islet were cultured in a modified culture medium (25): Minimum essential medium (#12492013; Thermo fisher) with 1× GlutaMAX (#17504044; Gibco), 11mM glucose, 5% FBS, 10 mM HEPES (#15630080; Thermo fisher) and 1× B-27 Supplement (#17504044; Gibco). Before transduction with lentivirus, islets were dissociated with a trypsin EDTA solution (#25200056; Thermo Fisher Scientific) for 3 min and cultured overnight. Islets were treated with 5μM Verteporfin (# SML0534; Sigma) or DMSO vehicle for 48hrs, and then continued to detect Ki67 signals by immunostaining.

Lentivirus packaging

8×10^6 HEK293T cells cultured in DMEM/10%FBS medium were incubated at 37°C, 5% CO_2 for 20 h. A mixture of the three-plasmid system [psPAX2 (1.3 pmol), pMD2.G (0.72 pmol), and transfer plasmid (1.64 pmol)] was prepared and transfected into 293T cells using Lipofectamine 3000 kit. After replenishment with antibiotics-free medium 12 h post-transfection, the lentivirus-contained medium was harvested at 48hrs post-medium-replenish and filtered throu gh a 0.45μm PES filter and further concentrated using Lenti-X Concentrator (#631232; Takara Bio) according to the manufacturer's instructions.

Annexin-PI apoptosis assay and EDU proliferation assay

HeLa cells were trypsinized into single cells and stained with Annexin-V (APC labeled), and Propidium Iodide for 15min at room temperature in the dark; cellular apoptosis was assessed by flow cytometry on BD LSRII, and data was analyzed on FlowJo software (TreeStar Inc). EDU (5-ethynyl-2′-deoxyuridine) was detected by the Click-iT Plus EDU flow cytometry Kit (#C10646; Thermo Fisher) according to the manufacturer's instructions. Briefly, EDU were incorporated in the culture medium at the final concentration of 10 μM for 1hr, followed by 15 min fixation and 15 min permeabilization. After 30 min incubation in 0.5ml Click-iT® Plus reaction cocktail, the cells were rinsed and analyzed using a flow cytometer.

GFP-positive cell counting and relative proliferation rate

To reduce the potential cytotoxicity from lentiviral transduction, the titers of lentiviruses were adjusted to achieve approximately 50% GFP-positive rate by 24 h post-transduction. Target-gene-P2A-GFP lentiviruses were transduced at the MOI of 1 into HeLa and NT2 cells, 0.5 into INS1 cells and 10 into INS2 cells. Flow cytometry was adopted to determine the percentage of GFP-positive cells. At different time points, GFP-positive rate was used to demonstrate the relative proliferation rate.

Immunostaining

Immunostaining was performed as previously described (24). Primary antibodies used were TEAD1 (#ab133533; rabbit polyclonal, Abcam), TEAD1 (#12292; rabbit monoclonal, Cell Signaling), Ki67 (#ab15580; rabbit polyclonal, Abcam), Insulin (#ab181547; rabbit monoclonal, Abcam), Insulin (#ab6995; mouse monoclonal, Abcam), Insulin (#PA1-26938; guinea pig ploYclonal, Thermo fisher), MAFA (#ab264418; Rabbit monoclonal, Abcam), GLUT2 (#ab54460; Rabbit polyclonal, Abcam), Proinsulin (#ab243141; mouse monoclonal, Abcam), YAP1 (#14074; rabbit monoclonal, Cell Signaling), NR4A3 (#sc-393902; mouse monoclonal, Santa Cruz Biotechnology). Tyramide SuperBoost Kits (#B40943; Thermo fisher) were used for YAP1 staining in the islets according to the manufacturer's instructions. The images were captured by the Nikon confocal microscope.

Western blotting

Western blotting was performed as previously described (22). The following antibodies were used: TEAD1 (#ab133533; Abcam), YAP1 (#14074; Cell signaling), NR4A3 (#sc-393902; Santa Cruz Biotechnology), WWC2 (#24750–1-AP; Proteintech), PKCiota (#NBP1-84959; Novus Biologicals), POLII (#NB200-598; Novus Biologicals), Myc-Tag (#2278; Cell signaling), α-tubulin (#3873; Cell signaling) and GAPDH (#MA1-16757; Thermo Fisher). The blots were imaged using Licor Odyssey Clx.

Realtime PCR

Total RNA was extracted and cleaned up using Direct-zol RNA Kit (#R2051; Zymo Research) according to manufacturer's protocol. Complementary DNA (cDNA) were synthesized using cDNA Synthesis Master Mix (#R6200; GenDEPOT). Realtime qPCR was carried out using amfisure qGreen qPCR Master Mix (#Q5603; GenDEPOT) in a Roche 480 Light Cycler machine. 18S or GAPDH served as an internal control. The qPCR primers were designed by IDT PrimerQuest Tool (https://www.idtdna.com/Primerquest/Home/Index) and checked if they span exon-exon junctions by CLC Sequence Viewer 8.

Luciferase assay

HOPFLASH reporter was a gift from Barry Gumbiner (26). We also subcloned 8x MCAT sequence from the original HOPFLASH into a lentiviral vector to facilitate islet transduction. The following sequences cloned from the promoter region were used to drive Firefly luciferase expression for luciferase reporter construction: human CTGF between −600 and 0, mouse YAP1 between −1400 and +660, human YAP1 between −500 and +400, human LATS2 between −420 and +100, human NR4A3 between −500 and +300, human TEAD3 between −900 and +250, human WWC2 between −450 and +450, human KNTC1 between −500 and +200, human PRKCI between −500 and +285, and human Ki67 between −1207 and +316. PCR and overlap PCR were performed using primers with the MCAT mutation and the mYAP1 reporter as a template to generate the ΔmYAP1 reporter. Luciferase assays were performed with a Dual-Luciferase® Kit (#E1960; Promega) according to the manufacturer's instructions. Renilla luciferase activities or total protein content served as internal controls. Total protein content was measured by the BCA method (#23225; Thermo Fisher). All reporter plasmids utilized in this study were validated by Sanger sequencing.

RNA-SEQ

Total RNA samples with RNA integrity number (RIN) ≥8 were used for transcriptome sequencing. For each group, two pooled islet RNA samples (10ng) isolated from one-year-old mice (three mice in each pooled sample; six mice in total) were amplified and synthesized into double-stranded cDNA, which were sheared into 200–300bp fragments and ligated with Illumina paired-end adaptors using the Illumina TruSeq DNA library preparation kit according to the manufacturer's instructions (Illumina, San Diego, CA). PCR amplification was performed to obtain the final cDNA library using Illumina kits. Bioanalyzer 2100 (Agilent Technologies, Santa Clara, CA) analysis was used to verify fragment size after amplification, library size, and concentration before clustering. A total of 10 pM of the library was then used for paired-end sequencing on the HiSeq 2500 at the Sequencing core at Brigham Young University. Further analyses were performed using the CLC genomics workbench 22. Raw reads were mapped to the mouse reference genome build 10 (UCSCmm10/GRCm38). Mapped reads were counted using the feature counts, and differential expression between the samples analyzed using multiple hypothesis testing. Significance was assessed by analyzing signal-to-noise ratio and gene permutations based on 1000 permutations. Molecular signature database (MSigDB) 3.0 curated gene sets for hallmark and canonical pathways were used for the analysis. Significant gene sets with enrichment score and a *q*-value cutoff of 0.05 are presented.

Chromatin immunoprecipitation (ChIP) assay

ChIP was performed with EZ-Magna ChIP™ HiSens Chromatin Immunoprecipitation Kit (#17-10461; Sigma) according to the manufacturer's instructions. Chromatin immunoprecipitations were performed using POLII antibody (# NB200-598; Novus Biologicals) or mouse IgG (#MAB002; R&D) in 293T and HeLa cells lysates. Immunoprecipitated DNA was then used as the template for qPCR. Primers, 5'-CGGACCGGATTAACCTTAGTG-3′ (CK1F), 5′- GCGAGGAATCGGGACAAC-3′ (CK1R), 5'- GGAGGAGTTGTGTTTGTGGA -3′ (CK2F), and 5′- CGATCTTTCCGCCCTTCTT-3′ (CK2R), were used to amplify POLII-bound DNA sequences. Primers, 5'-GGGCGCTTCTCCTAACTTT-3′, and 5'-GTTCCTTCCTTCCTCCCTTTC-3′, were used to amplify POLII-bound DNA sequences in the promoter region of YAP1 in HeLa cells. Primers, 5'-CATAAATGACGTGCCGAGAGA-3′, and 5'-CTGTGTGTGCGAGTGAGG-3′, were used to amplify POLII-bound DNA sequences in the promoter region of NR4A3 in HeLa cells.

TEAD1-ChIP sequencing

Frozen tissue sections were sent to Active Motif Services (Carlsbad, CA) for Chip-seq processing. In brief, the tissue section was submerged in 1% formaldehyde/PBS, chopped into small pieces, and incubated at room temperature for 15min. Fixation was stopped by the addition of 0.125M glycine (final). The tissue pieces were then treated with a Tissue Tearer and finally spun down and washed 2× in PBS. Chromatin was isolated by the addition of lysis buffer, followed by disruption with a Dounce homogenizer. Lysates were sonicated, and the DNA sheared to an average length of 300–500 bp. Genomic DNA (Input) was prepared by treating aliquots of chromatin with RNase, proteinase K, and heat for de-crosslinking, followed by ethanol precipitation. Pellets were resuspended, and the resulting DNA was quantified on a NanoDrop spectrophotometer. Extrapolation to the original chromatin volume allowed quantitation of the total chromatin yield. An aliquot of chromatin (10μg for islets) was precleared with protein G agarose beads (Invitrogen). Genomic DNA regions of interest were isolated using 20 μl TEAD1 antibody. Complexes were washed, eluted from the beads with SDS buffer, and subjected to RNase and proteinase K treatment. Crosslinks were reversed by incubation overnight at 65°C, and ChIP DNA was purified by phenol-chloroform extraction and ethanol precipitation. Quantitative PCR (qPCR) reactions were carried out in triplicate on specific genomic regions using SYBR Green Supermix (Bio-Rad). The resulting signals were normalized for primer efficiency by qPCR for each primer pair using Input DNA.

Illumina sequencing libraries were prepared from the ChIP-DNA and input DNAs by the standard consecutive enzymatic steps, including end-polishing, dA-addition, and adaptor ligation. The procedure was performed in an automated system (Apollo 342, Wafergen Biosystems/Takara). After a final PCR amplification step, the resulting DNA libraries were quantified and sequenced on Illumina's NextSeq 500 (75 nt reads, single end). Reads were aligned to the mouse genome (mm10) using the BWA algorithm (default settings). Duplicate reads were removed, and only uniquely mapped reads (mapping quality ≥ 25) were used for further analysis. Alignments were extended in silico at their 3'-ends to a length of 200 bp, which is the average genomic fragment length in the size-selected library, then assigned to 32-nt bins along the genome. The resulting histograms (genomic 'signal maps') were stored in bigWig files. Peak locations were determined using the MACS algorithm (v2.1.0) with a cutoff of P-value = 1e−7. Peaks that were on the ENCODE blacklist of known false ChIP-Seq peaks were removed. Signal maps and peak locations were used as input data to Active Motifs proprietary analysis program, which would output Excel files containing detailed information, including sample comparison, peak metrics, peak locations and gene annotations.

Published ChIP-seq and RNA-seq data accession and reanalysis

BED and WIG files were obtained from Chip-atlas (http://chip-atlas.org/) (27). WIG files were opened in UCSC Genome Browser (https://genome.ucsc.edu/) or integrative genomics viewer (IGV) to generate the 'peak' graphs. TEAD target gene information, such as 'peak score', annotation and nearby genes, were processed and obtained using CLC Genomics Workbench 22 (Qiagen). TEAD1 Chip-seq data in pancreatic progenitor cells were obtained from ArrayExpress (E-MTAB-1990 and E-MTAB-3061) (28).

Statistical analysis

The data are presented as means ± SEM. The *in vitro* data is representative of at least three independent experiments. Significance tests were determined by the two-tailed, unpaired Student's t-test, or two-way ANOVA followed by Sidak's multiple comparisons test. $p < 0.05$ was considered statistically significant and labeled with $*P < 0.01$, $**P < 0.001$, ***GraphPad Prism 7.04 software was used for statistical analyses and data graphing.

RESULTS

TEAD1 can repress tumor cell proliferation

Analysis of RNA-sequencing (RNA-seq) data from The Cancer Genome Atlas (TCGA) showed that TEAD1 was significantly reduced in 15 of 33 tumors compared with normal tissues (Figure 1A). In patients with clear cell renal cell carcinoma (KIRC), the survival rate with low TEAD1 expression was significantly reduced ($P < 0.001$), as indicated by analysis via Kaplan–Meier (KM) curves (Supplementary Figure 1A), suggesting TEAD1 may have anti-oncogenic effects. In this study, we generated a uniform lentiviral backbone to overexpress target genes (Supplementary Figure 1B), the advantage of which was that the GFP levels paralleled the target protein levels. TEAD1 overexpression had a strong effect on inhibiting the growth of HeLa (cervical cancer), NT2 (teratocarcinoma), and a moderate effect on PANC-1 (pancreatic ductal carcinoma) cells, while no significant effect was observed in 293T cells (Figure 1B, Supplementary Figure 1C). TEAD1 protein was successfully overexpressed by lentivirus, validated in 293T cells (Supplementary Figure 1D). In HeLa cells with TEAD1 overexpression, the percentage of EDU-positive cells was significantly reduced, as indicated by flow cytometry analysis (Figure 1C). In addition, cells going through early- or late-apoptosis stages were significantly increased with TEAD1 forced expression (Figure 1D). We next implanted HeLa cells into nude mice subcutaneously to evaluate the effects of TEAD1 overexpression on tumorigenesis. At 14 days after xenograft, the size of the tumors dissected was significantly smaller in TEAD1-overexpressing HeLa xenografts than in the controls (Figure 1E). This demonstrated that in many cell types that display high proliferation, especially cancer cell models, TEAD1 overexpression leads to a restriction on proliferation. However, whether TEAD1 also significantly restricted proliferation in adult differentiated cells with inherent low proliferation rates needed to be ascertained.

Conditional knockout of TEAD1 in pancreatic β cells results in cell-autonomous proliferation

To further investigate the role of TEAD1 on cell proliferation in vivo, we generated a β-cell conditional TEAD1

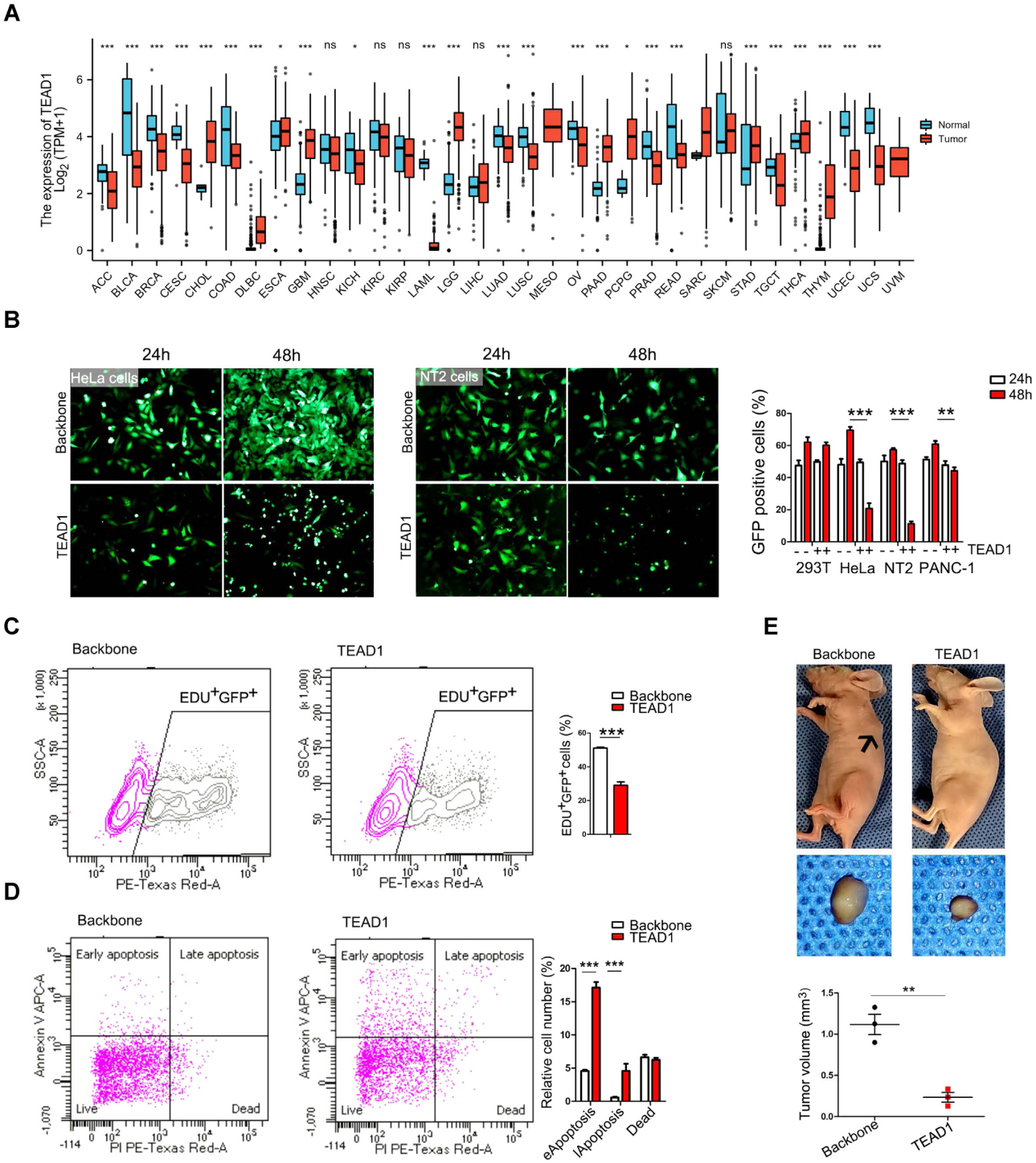

Figure 1. TEAD1 can repress cell proliferation in tumor cells. (**A**) TEAD1 transcript in 33 tumor lines and the adjacent normal tissues. (**B**) Visualization and quantification of cell growth in TEAD1 overexpressed cells by TEAD1-P2A (2A self-cleaving peptides)-GFP. (**C**) Quantification of cell proliferation by EDU incorporation assay. (**D**) Quantification of apoptosis and cell death by Annexin V and propidium iodide staining. (**E**) *In vivo* tumorigenesis in nude mice. The arrows show the tumor xenograft. $*P < 0.05$, $**P < 0.01$ and $***P < 0.001$; error bars represent standard error of the mean (SEM).

knockout (TKO) mouse model. Random blood glucose levels were significantly increased in TKO mice (Figure 2A). In isolated islets, Glucose-stimulated insulin secretion (GSIS) revealed that insulin secretion in response to 25 uM glucose stimulation was significantly reduced in TKO mice (Figure 2B). Immunostaining and Western analysis of islets indicated that TEAD1 was ablated selectively in β-cells in TKO mice (Figure 2C, D). Examination of proliferation via Ki67 detected significantly increased numbers of β-cells in TKO mice (Figure 2E). As hyperglycemia can also induce β-cell proliferation, we used an insulin pump to lower glucose levels to test whether the elevated proliferation of TKO β-cells is a cell-autonomous effect (Figure 2F). As expected, the Ki67-positive rate was lowest in mice receiving insulin and normal controls. However, it remained high in TKO with Insulin treatment compared to TKO receiving saline control (Figure 2G), suggesting that proliferation in TKO is not driven by the potential confounding effect of hyperglycemia but a direct consequence of loss of TEAD1 function. With the same insulin dose, TKO mice with an Insulin pump had the lowest non-fasting blood glucose level measured on Day 7 and Day 14 (Figure 2H). Fasting serum C-peptide levels were low in Con + insulin mice, but was significantly increased in both TKO + NaCl and TKO + insulin mice (Figure 2I), suggesting that the increase in β-cell proliferation after TEAD1 knockout is cell-autonomous and could not be repressed by treatment of hyperglycemia with exogenous insulin. Immunostaining showed that proinsulin was located close to the nucleus in control mice, while it spread throughout the cytoplasm in TKO mice, which could not be reversed by exogenous insulin treatment (Supplementary Figure 1D), suggesting that TEAD1 knockout resulted in reduced processing of proinsulin into mature insulin. Mature β-cell markers, MAFA and GLUT2, were also significantly reduced in TKO mice (Supplementary Figure 1E-F). Consistent with findings of increased Ki67-positive β-cells, the relative nuclear number in islets was higher in TKO islets compared to controls (Figure 2J and Supplementary Figure 1G), although relative insulin-positive areas were comparable (Figure 2K). These data collectively demonstrate that TEAD1 deletion in TKO β-cells increased cell-autonomous proliferation with immature phenotype.

This raised the interesting question of whether TEAD1 also played a role in β cells that already have an increase in proliferation, such as in insulinoma-derived INS2 cells. In INS2 cells with TEAD1 overexpression, EDU-positive cells were markedly lower than the controls (Figure 2L), indicating that TEAD1 gain-of-function in β-cell suppresses proliferation consistent with the loss-of-TEAD1 function leading to increased β-cell proliferation in TKO islets.

Screening of TEAD1 target genes

β-cells of TKO display some phenotypic characteristics of immature neonatal β-cells, including impaired glucose-stimulated insulin secretion (GSIS) and a high rate of proliferation (29). To identify potential target genes directly repressed by TEAD1, we examined genes upregulated in the TKO islets that were also identified as direct TEAD1 target genes in β-cell progenitors. Among 955 up-regulated genes in the TKO RNA-seq data with a fold change >2 and adjusted *P*-value <0.05 as compared to controls, we found 59 genes overlapped with TEAD1 target genes identified by ChIP-seq in pancreatic progenitor cells (Figure 3A). Since the proximity of the binding site to the transcription start site (TSS) is strongly correlated to the strength of the regulation by the transcription factor (30), among the 59 genes, we selected 8 potential TEAD1 target genes (TTG), based on regulatory sequence proximity to TSS (<1000 bp), for detailed functional analysis: NR4A3, WWC2, YAP1, Amotl2, KNTC1, LATS2, PRKCI and WTIP. We also noticed that a TEAD1 binding peak was observed in the promoter region of TEAD3, although the fold change of TEAD3 was 1.3 in the TKO RNA-seq (Figure 3B). TEAD1 binding peaks were identified in these genes in pancreatic progenitor ChIP-seq analysis (Figure 3C). Furthermore, we performed ChIP-seq using wild-type mouse islets, and TEAD1 binding peaks were also identified within the promoter regions of WWC2, NR4A3, Amotl2 and LATS2 (Figure 3D). As RNA-seq was performed using islets from 1-year-old mice, TTG expression levels were also assessed in young mouse islets. All TTGs analyzed except PRKCI were significantly increased in 3-month-old TKO islets (Figure 3E). As YAP is a key effector in the Hippo pathway for the co-activation of TEAD, it was intriguing that YAP1 was identified as a TEAD1 direct target gene in β-cells. Analysis of YAP1 promoter demonstrated the presence of three MCAT motifs located close to the TSS in mouse YAP1, and an MCAT was found in the human YAP1 promoter region. TEAD-binding motifs were also present near TSS in mouse and human TEAD3 promoters (Supplementary Figure 2A), as were the other TTGs identified (Supplementary Figure 2B). To test whether TEAD1 regulation of its target genes was MCAT motif orientation/strand dependent, two constructs of the promoter of human CTGF, a known TEAD1 target, were used to generate luciferase reporters, one containing the two endogenous MCAT element (hCTGF) and the other with two MCAT in a reversed orientation (ΔhCTGF). Luciferase activity was comparable between hCTGF and ΔhCTGF (Figure 3F), suggesting that TEAD1 DNA binding and transcription via the MCAT motif was not orientation dependent. Furthermore, we generated a luciferase reporter to directly test TEAD1 regulation of YAP1 using the sequence between −1300 and +660 of mouse YAP1 (mYAP1r). A luciferase assay showed that TEAD1 repressed YAP1 promoter activity in the basal state, as indicated by mYAP1r. When co-expressed with YAP5SA (a constitutively active form of YAP) or VGLL4 (a co-repressor), YAP1 promoter activity was significantly promoted or further repressed, respectively (Figure 3G). The TEAD1 protein pocket region is known for mediating co-activator/co-repressor interaction, including YAP, TAZ and VGLL4, to drive the transcription response. To determine whether the TEAD1-mediated repression mechanism that we observed depends on its pocket region, we generated a truncated TEAD1 (ΔTEAD1) with deletion of aa 358–426 to disrupt the binding of pocket structure with co-regulators. A split-GFP system (31), particularly suited to studying protein-protein interactions via live cell imaging, was adopted to determine ΔTEAD1 interaction with YAP1, TAZ and VGLL4. In this study, we present a modified split-GFP system that has

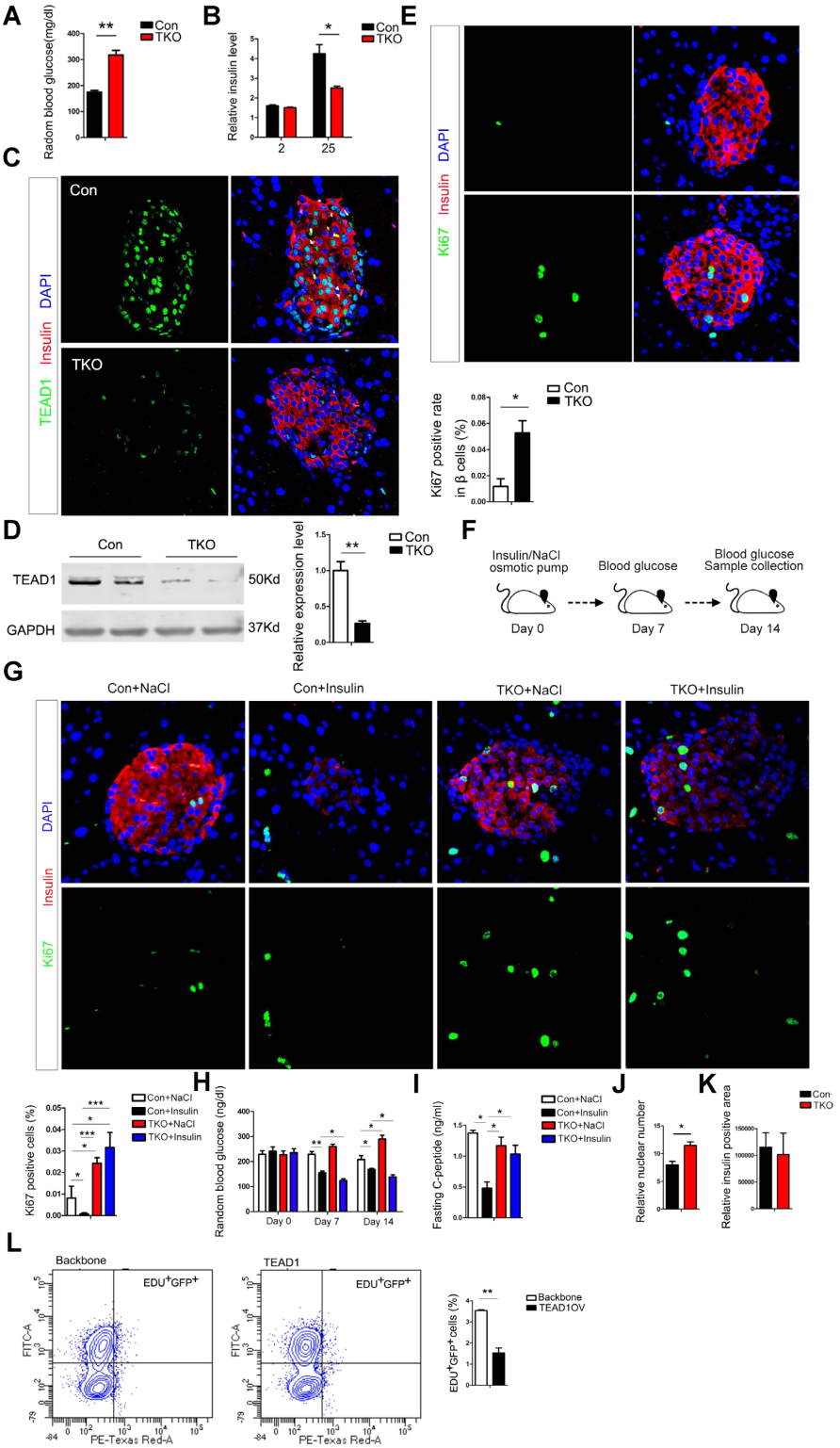

Figure 2. TEAD1 ablation in pancreatic β cells induces proliferation and an immature phenotype. (**A**) Random blood glucose levels in β-cell specific TEAD1 knockout (TKO) mice. (**B**) Glucose (2 mM versus 25 mM) induced insulin secretion in mouse islets isolated from TKO and control mice. (**C**) TEAD1 immunostaining on pancreas sections from TKO and control mice. (**D**) Immunoblotting using pancreatic islet lysates isolated from TKO and control mice. (**E**) Ki67 staining and quantification on pancreas sections from TKO and control mice. (**F**) Experimental scheme for insulin pump implantation. (**G**) Ki67 staining and quantification on pancreas sections from insulin pump implanted TKO or control mice. (**H**) Random blood glucose levels on dpi (days post insulin pump implantation) 7 and 14. (**I**) Fasting C-peptide levels on dpi 14. (**J**) Nuclei quantification per islet in TKO and control mice. (**K**) Relative insulin-positive area (insulin positive area / total area of the pancreas) analysis in TKO and control mice. Total of 32 pancreatic sections from four TKO and four control mice were analyzed. (**L**) Quantification of cell proliferation by EDU incorporation assay in TEAD1-overexpressed mouse INS2 insulinoma line. $^{*}P < 0.05$, $^{**}P < 0.01$ and $^{***}P < 0.001$; error bars represent SEM. Con, control.

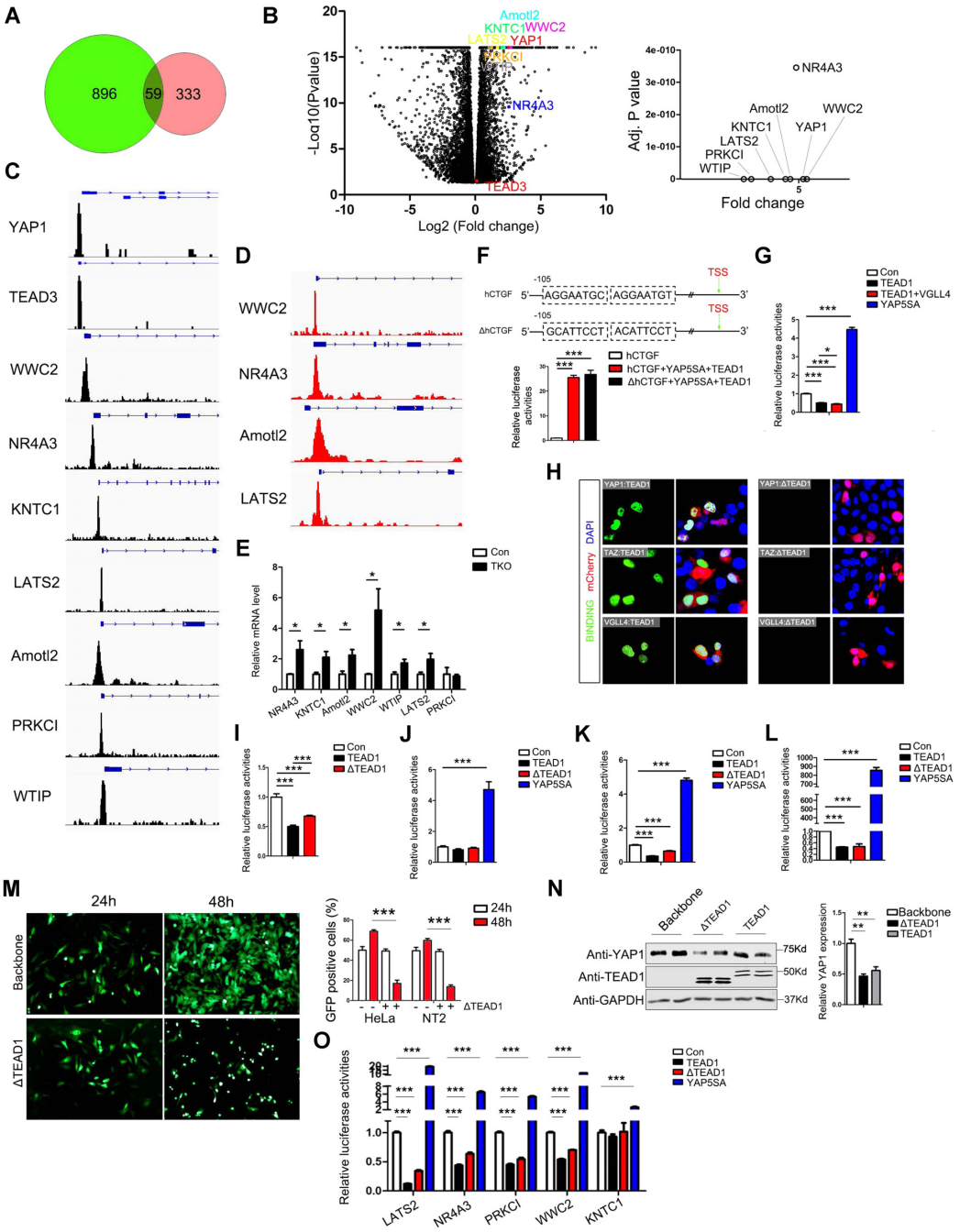

Figure 3. The identification of bona fide TEAD1 target genes. (**A**) Venn graph showing potential TEAD1 targets (59 genes) by cross-referencing TKO RNA-seq (955 upregulated genes) and TEAD1-ChIP-seq (392 genes) datasets. (**B**) Narrowing down to nine TEAD1 direct target genes (TTG) based on regulatory sequence proximity to transcription start sites (TSS) (<1000 bp). (**C**) TEAD1-ChIP-seq in pancreatic progenitor cells showing strong TEAD1-bound signals that are close to TSS of the candidate TTGs. (**D**) TEAD1-ChIP-seq in wild-type mouse islets showing TEAD1-bound signals that are close to TSS on WWC2, NR4A3, Amotl2, and LATS2 genes. (**E**) Quantitative PCR showing the expression of TTGs in TKO and control islets isolated from 12-week-old male mice. (**F**) Illustration of human CTGF promoter (hCTGF) driven luciferase reporter and mutant human CTGF promoter (ΔhCTGF) driven luciferase reporter on which the MCAT motif was moved to the reverse strand. A luciferase assay showing no difference in activity between ΔhCTGF and hCTGF promoters with co-transfection of YAP5SA and TEAD1. (**G**) Luciferase assays using mouse YAP1 promoter reporter (mYAP1r) show that TEAD1 and TEAD1 + VGLL4 repress YAP1 transcription, while YAP5SA promotes YAP1 transcription. (**H**) Split-GFP system showing no binding as indicated by GFP signal between ΔTEAD1 (truncated TEAD1) and YAP1/TAZ/VGLL4. mCherry signal indicate transfection efficiency. Nuclei were counterstained with diamidino-2-phenylindole (DAPI) (blue). (**I**) mYAP1r-promoter luciferase assays show both TEAD1 and ΔTEAD1 repress YAP1 transcription. (**J**) ΔmYAP1r (MCATs mutant)-promoter luciferase assays show absent repression of YAP1 transcription by TEAD1 or ΔTEAD1 whereas YAP5SA transcriptional activation of YAP1 is impaired. (**K**) Human YAP1 promoter and (**L**) Human TEAD3 promoter luciferase assays show TEAD1 and ΔTEAD1 repression and YAP5SA activation of transcription. (**M**) ΔTEAD1 inhibit HeLa cell growth. GFP positivity demonstrate ΔTEAD1 or backbone (empty vector) lentiviral transduction. (**N**) YAP1 protein expression by Western blotting after TEAD1 and ΔTEAD1 overexpression in Hela cells. (**O**) Human TTGs promoter luciferase assay show TEAD1 and ΔTEAD1 repress the transcription of most TTGs except KNTC1, while YAP5SA promotes the transcription of all TTGs. $*P < 0.05$, $**P < 0.01$ and $***P < 0.001$; error bars represent SEM.

improved sensitivity and overcomes inefficiencies (Supplementary Figure 2C). As compared to full-length TEAD1, ΔTEAD1 failed to bind YAP1, TAZ or VGLL4, as indicated by the split-GFP system (Figure 3H), suggesting that the pocket region is critical for the binding of TEAD1 and its cofactors, as expected. Western blotting confirmed that ΔTEAD1, YAP1, TAZ and VGLL4 were expressed properly in the split-GFP system (Supplementary Figure 2D). Surprisingly, ΔTEAD1, when transfected with mYAP1r promoter, was able to repress YAP1 transcription similarly as the full-length TEAD1 (Figure 3I). To determine whether TEAD1 repression depends on MCAT, we mutated all three motifs in mYAP1r (ΔmYAP1r). TEAD1 or ΔTEAD1 could no longer repress transcription of ΔmYAP1r, but YAP5SA still induced luciferase activity (Figure 3J), suggesting that YAP5SA can function in a TEAD-independent manner. Furthermore, we obtained similar results using human YAP1 and TEAD3 promoter regions (hYAP1r and hTEAD3r) (Figure 3K–L), suggesting that a similar mode of TEAD pocket-independent repression mechanism was conserved between human and mouse promoter regulation. In HeLa cells, ΔTEAD1 inhibited cell growth similarly observed with the full-length TEAD1 (Figure 3M). YAP1 expression was significantly reduced in TEAD1 and ΔTEAD1-overexpressing HeLa cells (Figure 3N). We further screened all the TTG promoter regions, including LATS2, NR4A3, PRKCI, WWC2 and KNTC1 via luciferase reporters, and found that LATS2, NR4A3, PRKCI, and WWC2, can be similarly repressed by both TEAD1 and ΔTEAD1 and induced by YAP5SA. KNTC1 was not repressed by TEAD1 or ΔTEAD1, although it can be activated by YAP5SA (Figure 3O). Similarly, CTGF cannot be repressed by TEAD1, while TEAD1 + VGLL4 can repress its expression (Supplementary Figure 2E). Collectively, these results revealed two regulatory mechanisms involved in TEAD1 transcription control in distinct subsets of target genes. One set of genes is repressed by TEAD1 directly in a pocket-area-independent manner, as represented by LATS2, NR4A3, PRKCI and WWC2, while another set, such as KNTC1 and CTGF, requires TEAD1 cofactor binding.

Function validation of TTGs

Certain TTGs, such as LATS2, WWC2, Amotl2 and WTIP, were reported to have functions in regulating the Hippo pathway (32–35). To determine the potential roles of these TTG on TEAD1 activity, we used lentiviral expression and validated their protein levels (Supplementary Figure 3A). Interestingly, we found that WWC2 inhibited, while Amotl2, WTIP and YAP5SA activated TEAD1 pathway activity, as indicated by the HOPFLASH reporter (Figure 4A), suggesting that these target genes of TEAD1, together with additional components of Hippo-TEAD1 pathway, form a potential feedback regulatory loop to maintain the homeostasis of this pathway. We further interrogated the roles of these TTGs in modulating proliferation using a luciferase reporter driven by a human Ki67 promoter (hKi67r) (Figure 4B). YAP5SA significantly promoted Ki67 promoter transcription, while PKCiota (encoded by the PRKCI gene), Amotl2, WTIP and WWC2 repressed this activity (Figure 4C). Following forced expression of WWC2 and Amotl2, HeLa cells rounded up and detached at 48 hours, suggesting WWC2 and Amotl2 play important roles in the apoptosis process in HeLa cells (Supplementary Figure 3B). EDU-positive cells were markedly induced by YAP5SA but reduced by overexpression of WTIP, PKCiota, WWC2, Amoltl2 and NAR4A3 (Figure 4D). Similar effects of these genes were obtained in INS2 cells (Figure 4E). Given that the TEAD1 binding peak was identified in NR4A3 promoter in both pancreatic progenitor cells and mature β cells, NR4A3 may play important roles in β-cell differentiation and proliferation. There are two isoforms of NR4A3, full-length (NR4A3L) and truncated (NR4A3S) (Figure 4F), both of which are widely expressed (36–37). NR4A3 functions in β-cell proliferation remain controversial while the truncated isoform is yet to be studied (38–39), and NR4A3L and NR4A3S share the same promoter. In TKO islets, both NR4A3L and NR4A3S were up-regulated (Figure 4G). Furthermore, in INS2 cells, TEAD1 forced expression induced Ins1 and Ins2 expression, while Ki67, NR4A3L and NR4A3S were suppressed (Figure 4H). Immunostaining showed that Ki67-positive β cells were significantly reduced after overexpression of NR4A3L or NR4A3S in mouse islets (Figure 4I). NR4A3L and NR4A3S were robustly expressed using lentiviral transduction in normal mouse islets (Supplementary Figure 3C). In INS1 cells, its growth was inhibited by NR4A3L and NR4A3S (Supplementary Figure 3D). In INS2 cells, both NR4A3L and NR4A3S repressed Ki67 and markers of differentiated function such as Ins1, Ins2, and PDX1 expression, while both induced NKX6.1. NR4A3S, but not NR4A3L, also up-regulated UCN3 (another marker of mature β-cells), a β-cell maturation marker (Figure 4J). Thus two NR4A3 isoforms have broadly similar transcription repression functions in primary islets and β-cell lines, while they might exert distinct regulation in β-cell differentiation. Analysis of public RNA-seq data (GSE86924) revealed that NR4A3 loss-of-function led to inductions of Ki67 and INS in human β cells (Supplementary Figure 3E). We also co-expressed YAP5SA with other TTGs in HeLa cells at a 1:1 ratio to examine the net proliferation effects. YAP5SA promoted proliferation, while WTIP, WWC2, Amotl2, PKCiota and NR4A3 antagonized its proliferative effect, as indicated by the hKi67r-driven luciferase assay (Figure 4K).

YAP1 expression was reactivated after TEAD1 knockout in β-cells

YAP1 is not expressed in adult β-cells. Interestingly, RNA-seq revealed that YAP1 and TEAD3 expression were significantly induced in TKO β cells, and YAP1 protein was markedly elevated in TKO islets compared to a nearly undetectable level in controls (Figure 5A). A few YAP1-positive β cells were observed after TEAD1 knockout, as shown by immunostaining (Figure 5B). Since YAP1 stimulates robust cell proliferation of human islets (40), elevated YAP1 levels may contribute in part to the induction of β-cells proliferation in TKO mice. To test this, we used verteporfin (41) to block YAP1 function in TKO islets ex vivo and found that β cells positive for Ki67 were significantly reduced (Figure

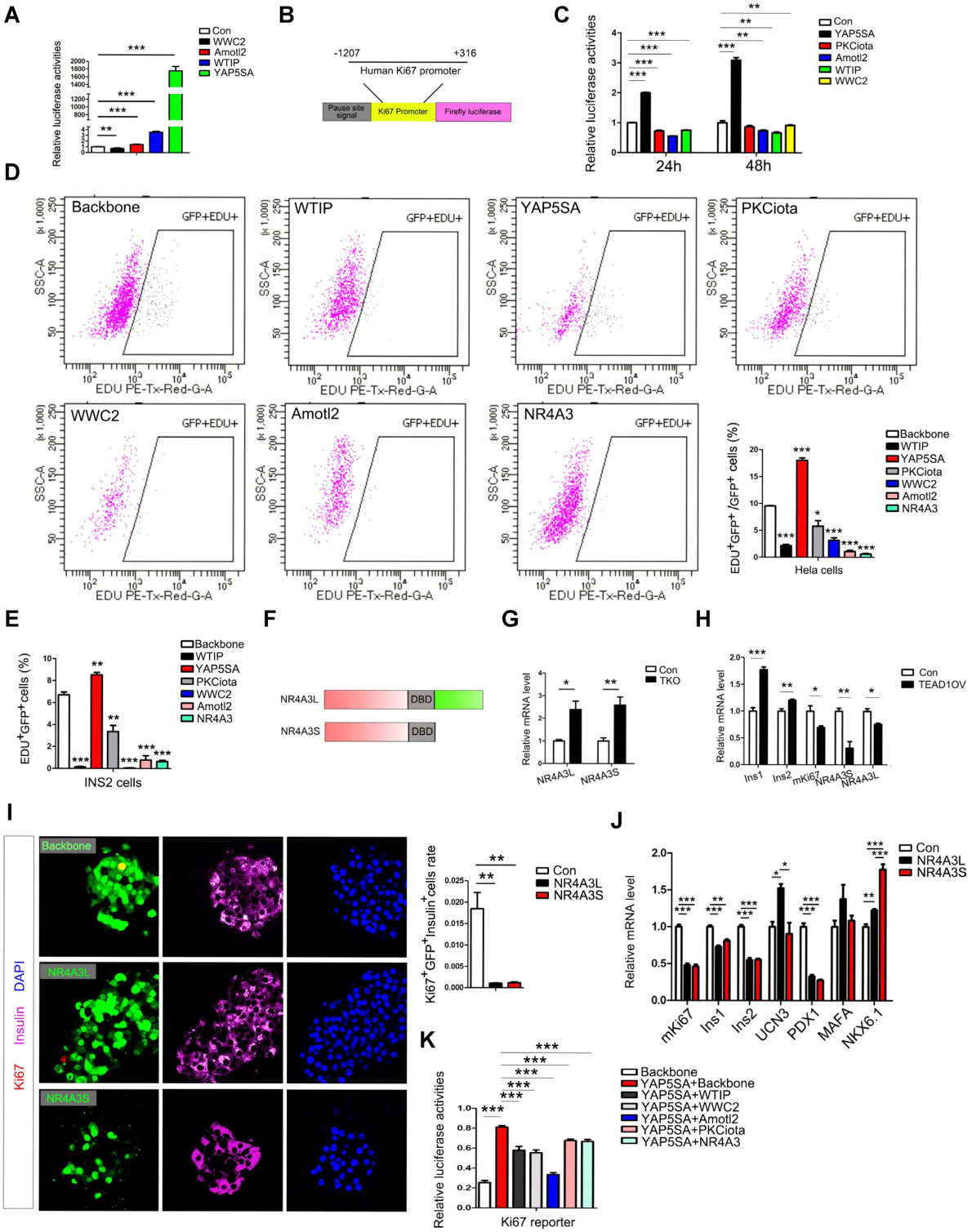

Figure 4. Function validation of TTGs. (**A**) HOPFLASH reporter luciferase assay show WWC2, AMOTL2, WTIP and YAP5SA regulation of Hippo signaling activity. (**B**) Human Ki67-promoter reporter (hKi67r) construct. (**C**) hKi67r reporter activities suggest differential regulatory effects of proliferation by TTGs. (**D**) Flow cytometry analysis of proliferative (EDU+) HeLa cells after TTGs overexpression (GFP+); double positives are indicated by grey dots. (**E**) Quantification of flow cytometry analysis in TTGs overexpressed INS2 cells. (**F**) Schematic representation of NR4A3 isoforms: NR4A3L, full-length NR4A3; NR4A3S, short form of NR4A3. (**G**) Quantitative PCR showing NR4A3L and NR4A3S mRNA expression in TKO islets. (**H**) Quantitative PCR showing Ins1, Ins2, Ki67, NR4A3L and NR4A3S mRNA expression in INS2 cells after TEAD1 overexpression (TEAD1OV). (**I**) Immunostaining and quantification of Ki67 + Insulin + cells in NR4A3L- and NR4A3S-overexpressing mouse islets. (**J**) Quantitative PCR showing Ki67, Ins1, Ins2, PDX1, MAFA and UCN3 mRNA expression in NR4A3L- and NR4A3S-overexpressed INS2 cells. (**K**) hKi67r reporter activity show WTIP, WWC2, AMTOL2, PKCiota and NR4A3 antagonize the proliferation effect of YAP5SA while co-transfecting with YAP5SA at a 1:1 molar ratio in HeLa cells. $*P < 0.05$, $**P < 0.01$ and $***P < 0.001$; error bars represent SEM.

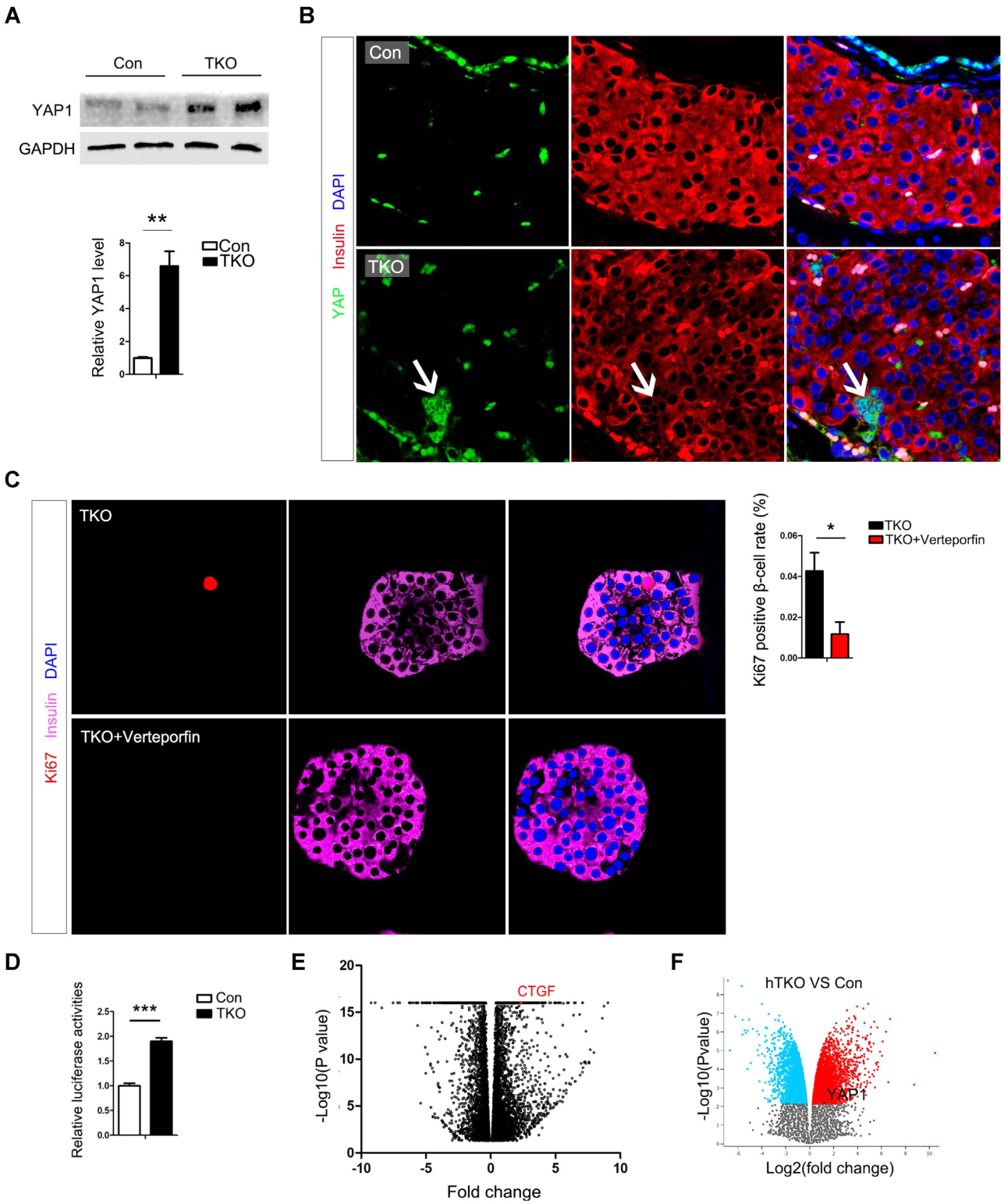

Figure 5. TEAD1 knockout in mouse pancreatic β cells results in elevated YAP1 expression. (**A**) Western blotting demonstrating YAP1 expression in TKO mouse islets. (**B**) Detection of YAP1 expression on TKO and control mouse pancreas sections (the arrows indicate YAP1 nuclear staining). (**C**) Immunostaining on isolated TKO islets showing *ex vivo* verteporfin effects on proliferation, with quantification showing in the bar chart. (**D**) Luciferase promoter assay showing TEAD pathway activities in TKO islets. (**E**) Volcano plot highlighting CCN2 (CTGF) transcript expression in TKO islets. (**F**) Volcano plot highlighting YAP1 transcript expression in the myocardium of TEAD1 cardiomyocyte-specific knockout mice. $^{*}P < 0.05$, $^{**}P < 0.01$ and $^{***}P < 0.001$; error bars represent SEM.

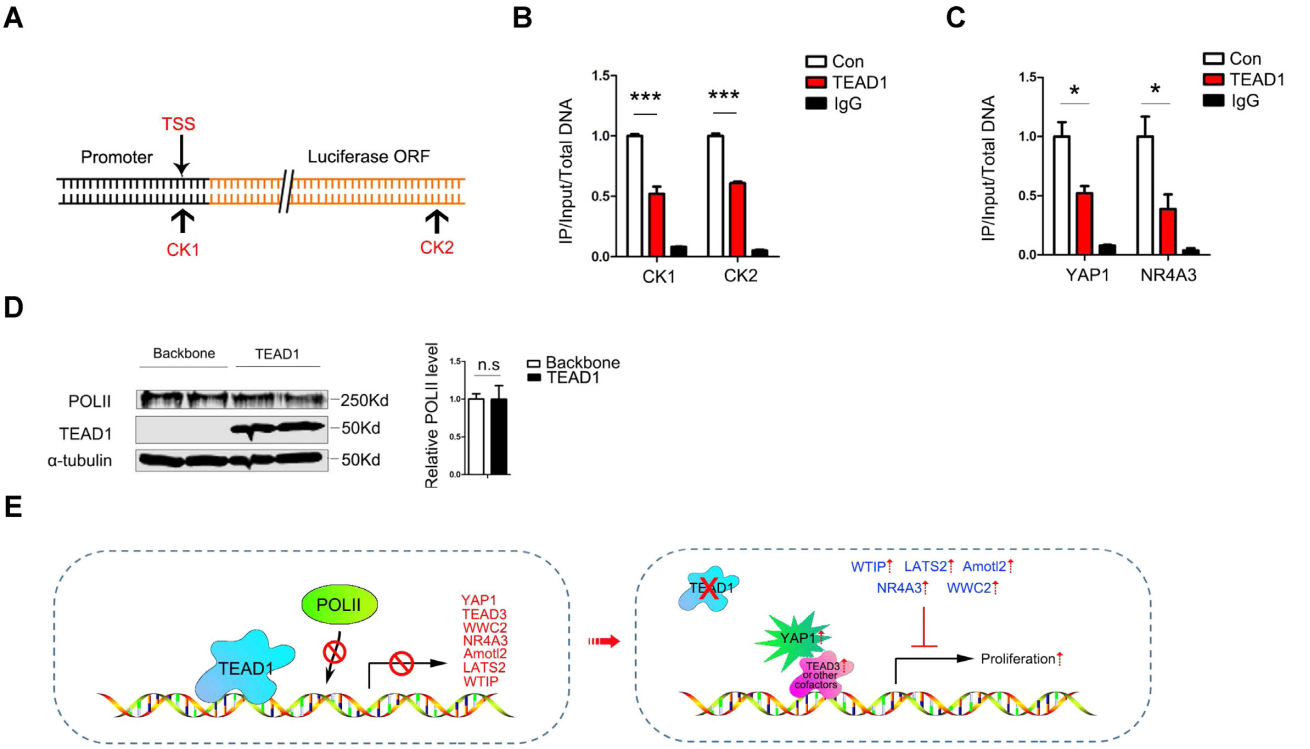

Figure 6. TEAD1 prevents RNA-polymerase II (POLII) from binding to DNA. (**A**) Two potential POLII binding sites (checkpoints, CK) in YAP1 reporter vector were chosen to perform POLII-ChIP experiments. (**B**) ChIP assay showing lower POLII binding on the two CKs after TEAD1 overexpression. (**C**) ChIP assay showing lower POLII binding on the endogenous YAP1 and NR4A3 promoter region after TEAD1 overexpression in HeLa cells. (**D**) Western blotting showing POLII expression in TEAD1-overexpressing or empty vector transduced HeLa cells. (**E**) Schematic representation showing the TEAD1-TTG regulatory loop in pancreatic β cells. $*P < 0.05$, $**P < 0.01$ and $***P < 0.001$; error bars represent SEM.

5C), demonstrating that YAP1 induction by loss of TEAD1 contributes to increased β-cell proliferation. TEAD pathway activities were enhanced in TKO islets, as indicated by the HOPFLASH reporter (Figure 5D) in islets, which could be due to signaling activation through other TEADs with YAP1 induction. This finding is in line with RNA-seq, indicating that CTGF, the canonical target gene in the Hippo pathway implicated in β-cell proliferation (42), was significantly increased in TKO islets (Figure 5E). In our previous study with TEAD1 ablation in cardiomyocytes (15), YAP1 expression was also increased (Figure 5F). Together, these data indicate that TEAD1 deletion led to a re-expression of YAP1, suggesting a de-repression of TEAD1-mediated repression of YAP1 in adult β-cells that was correlated with an increase in β-cell proliferation.

TEAD1 can repress RNA polymerase II (POLII) DNA binding

Since the MCAT motif was close to the TSS in TTGs (–100 bp to +400 bp), we hypothesized that TEAD1 might affect POLII-TSS binding to reduce the transcription of these TEAD1-repressed target genes. We selected two positions henceforth referred to as checkpoints (CKs), one close to the TSS and the other at the downstream site of mYAP1r (Figure 6A). After sonication, the lengths of most DNA fragments were 200–500 bp (data not shown). ChIP experiments showed that TEAD1 repressed POLII-DNA binding on both CK1 and CK2 (Figure 6B) when TEAD1 and mYAP1r were overexpressed in 293T cells. Similarly, ChIP showed that TEAD1 repressed POLII-DNA binding to the endogenous TSS region of YAP1 and NR4A3 after TEAD1 overexpression in HeLa cells (Figure 6C). We also show that TEAD1 does not repress POLII expression directly (Figure 6D).

In summary, TEAD1 restricted proliferation in distinct cancer cell lines and mature differentiated β-cells with low proliferation potential. Mechanistically TEAD1 repressed a set of TTGs, including YAP1, in mature β cells to restrict proliferation (Figure 6E) in a pocket-independent manner.

DISCUSSION

The hippo-TEAD1 pathway has been closely linked to tumorigenesis, with increased Yap-TEAD1 activity leading to malignant proliferation. Inhibitors of YAP, TEAD, or the YAP-TEAD interaction are being developed for cancer therapy (43). In this study, we uncovered a surprising effect of TEAD1 overexpression on suppressing tumor cell growth, while loss of TEAD1 results in enhanced cell proliferation in a non-tumor model of mature pancreatic β-cells. Recent studies identified feedback loops in the Hippo pathway involving YAP and TEAD, especially related to tumorigenesis (44–46). In this study, we screened all TEAD1 target genes and found a negative feedback regulatory loop mediated by TEAD1's repressive activity. However, the strength of TEAD1 repression was dependent on cell type, so the

repression effect of TEAD1 may also be tumor-cell type dependent.

In vascular smooth muscle cells, TEAD1 was found to be induced following arterial injury, and its overexpression can repress the smooth muscle-specific genes, including smooth muscle α-actin (16). In the heart, TEAD1 overexpression promotes age-dependent dysfunction by regulating target genes, including SERCA2a, p-CX43, p-GSK3/β, GATA4 and NFATc3/c4 (47). However, whether these are directly controlled by TEAD1 or secondary changes, such as regulation via TEAD1 cofactors, YAP1, TAZ and VGLL4, remains unclear.

Although TEAD1-4 are evolutionarily conserved, each TEAD factor has tissue-specific roles (48). ChIP-seq analysis of C2C12 myoblasts demonstrated that TEAD4 occupancy of 2940 sites was predominantly distant from TSS, while TEAD1 had only 1400 binding sites. Interestingly myoblast differentiation involved a switch from TEAD1 and TEAD4 occupancy in proliferating progenitors to predominantly TEAD4 binding in differentiated myocytes (49), suggesting that different TEAD factors regulate distinct targets. Compared to TEAD1, TEAD2-4 have low expression in β-cells; thus, β cells are particularly suited for studying TEAD1 regulation.

In mature β cells, YAP1-TEAD1 pathway activity is minimal due to the absence of YAP expression. TEAD1 loss-of-function leads to distinct findings in β cells compared to cardiomyocytes and most cancer cell lines. In cardiomyocytes, TEAD1 ablation decreased YAP1-TEAD1 pathway activity with reduced proliferation. In contrast, loss of TEAD1 increased YAP1-modulated transcriptional activity in β cells. This specific effect and mechanism in β-cells suggest a unique approach to reactivate proliferation for potential diabetes disease applications. YAP1-positive β-cell clusters were observed in the periphery TKO islets, although the lineage or identity of these cells, whether via transdifferentiation from other islet lineages, such as delta cells, or dedifferentiated from β-cells, warrants further study.

TEAD1-suppressed genes that we identified in this study share a common characteristic of having the MCAT elements close to TSS. Since TEAD1 has a relatively weak repression effect, as indicated by the 8x MCAT-driven synthetic HOPFLASH reporter, the outcome of TEAD1-MCAT binding is context-dependent. YAP1 and CTGF promote proliferation, while the TTGs we examined mainly antagonize this effect of YAP1. Overexpression of YAP1 promotes islet proliferation (40); however, YAP1 has potential oncogenic effects, limiting its translational potential. Our study demonstrates that blocking TEAD1-DNA binding may be a novel approach to reactivate β-cell proliferation, although its efficacy and safety will need further investigation. Transient blocking of TEAD1-DNA binding to reactivate β-cell proliferation with subsequent maturation with the restoration of TEAD1 activity could be a potential route to achieve an increase in functional β-cell mass. To translate this, identifying a reversible TEAD1 inhibitor could be crucial. The pocket area lies within the C-terminus of TEAD1, which is targeted by currently available inhibitors. Inhibitors of the three α-helices within the N-terminus of TEAD1 (50) could be important in modulating TEAD1 action, given our findings of the pocket-area-independent TEAD1 function. Recently, Aptamers were reported to be ideal candidates for diagnostic and therapeutic applications (51). Screening and finding a stable Aptamer with high binding affinity may enable 'sequential therapy' targeting TEAD1 to promote β-cell functional mass, while dCas9-mediated activation of specific TEAD1-binding MCAT elements may have value in restricting tumor proliferation.

In conclusion, the identification of this TEAD1-mediated orientation and a pocket-independent repressive mechanism that is generally applicable to malignant and non-malignant cell proliferation will lead to a better mechanistic understanding of physiological compensation in diseases such as diabetes and tumorigenesis.

DATA AVAILABILITY

All the raw and analyzed data files for the RNA-seq and ChIP-seq data presented are deposited in GEO. The tokens for access to data deposited in GEO: Expression data—GSE139228 (olwxaysirjybtgn) and GSE139152 (evevygymzfylhkv) and Chip-Seq data—GSE157513 (qxazkssgdnkdzsl).

SUPPLEMENTARY DATA

Supplementary Data are available at NAR Online.

ACKNOWLEDGEMENTS

Author contributions: F.L.: project design, performing experiments, data acquisition and analysis, manuscript preparation. V.N. and P.Y.: cell culture and islet isolation. J.L.: model generation, animal experiments, RNA-seq and ChIP-Seq. K.M. Manuscript preparation. M.M.: funding acquisition, data analysis, and manuscript preparation. V.Y.: project design, funding acquisition, project administration, data analysis, manuscript preparation.

FUNDING

VA-ORD [I01BX002678 to V.Y.]; National Institutes of Health [R01 DK130499 to V.Y.]; National Institutes of Health [R01-HL147946 to M.M.]. Funding for open access charge: Federal grants.

Conflict of interest statement. None declared.

REFERENCES

1. Yu,F. and Guan,K. (2013) The hippo pathway: regulators and regulations. *Genes Dev.*, **27**, 355–371.
2. Zhao,B., Ye,X., Yu,J., Li,L., Li,W., Li,S., Yu,J., Lin,J., Wang,C., Chinnaiyan,A. *et al.* (2008) TEAD mediates YAP-dependent gene induction and growth control. *Genes Dev.*, **22**, 1962–1971.
3. Zhang,H., Liu,C., Zha,Z., Zhao,B., Yao,J., Zhao,S., Xiong,Y., Lei,Q. and Guan,K. (2009) TEAD transcription factors mediate the function of TAZ in cell growth and epithelial-mesenchymal transition. *J. Biol. Chem.*, **284**, 13355–13362.
4. Lin,K.C., Park,H.W. and Guan,K. (2017) Regulation of the hippo pathway transcription factor TEAD. *Trends Biochem. Sci.*, **42**, 862–872.
5. Deng,X. and Fang,L. (2018) VGLL4 is a transcriptional cofactor acting as a novel tumor suppressor via interacting with TEADs. *Am. J. Cancer Res.*, **8**, 932–943.

6. Kim,M., Kim,T., Johnson,R. and Lim,D. (2015) Transcriptional co-repressor function of the hippo pathway transducers YAP and TAZ. *Cell Rep.*, **11**, 270–282.
7. Kaan,H.Y.K., Chan,S.W., Tan,S.K.J., Guo,F., Lim,C., Hong,W. and Song,H. (2017) Crystal structure of TAZ-TEAD complex reveals a distinct interaction mode from that of YAP-TEAD complex. *Sci. Rep.*, **7**, 2035.
8. Jiao,S., Wang,H., Shi,Z., Dong,A., Zhang,W., Song,X., He,F., Wang,Y., Zhang,Z., Wang,W. *et al.* (2014) A peptide mimicking VGLL4 function acts as a YAP antagonist therapy against gastric cancer. *Cancer Cell*, **25**, 166–180.
9. Kaneda,A., Seike,T., Danjo,T., Nakajima,T., Otsubo,N., Yamaguchi,D., Tsuji,Y., Hamaguchi,K., Yasunaga,M., Nishiya,Y. *et al.* (2020) The novel potent TEAD inhibitor, K-975, inhibits YAP1/TAZ-TEAD protein-protein interactions and exerts an anti-tumor effect on malignant pleural mesothelioma. *Am. J. Cancer Res.*, **10**, 4399–4415.
10. Lu,T., Li,Y., Lu,W., Spitters,T., Fang,X., Wang,J., Cai,S., Gao,J., Zhou,Y., Duan,Z. *et al.* (2021) Discovery of a subtype-selective, covalent inhibitor against palmitoylation pocket of TEAD3. *Acta Pharm. Sin. B.*, **11**, 3206–3219.
11. Mélin,L., Abdullayev,S., Fnaiche,A., Vu,V., Suárez,N.G., Zeng,H., Szewczyk,M.M., Li,F., Senisterra,G., Allali-Hassani,A. *et al.* (2021) Development of LM98, a small-molecule TEAD inhibitor derived from flufenamic acid. *ChemMedChem.*, **16**, 2982–3002.
12. Holden,J.K., Crawford,J.J., Noland,C.L., Schmidt,S., Zbieg,J.R., Lacap,J.A., Zang,R., Miller,G.M., Zhang,Y., Beroza,P. *et al.* (2020) Small molecule dysregulation of TEAD lipidation induces a dominant-negative inhibition of hippo pathway signaling. *Cell Rep.*, **31**, 107809.
13. Liu-Chittenden,Y., Huang,B., Shim,J.S., Chen,Q., Lee,S.J., Anders,R.A., Liu,J.O. and Pan,D.J. (2012) Genetic and pharmacological disruption of the TEAD-YAP complex suppresses the oncogenic activity of YAP. *Gene Dev.*, **26**, 1300–1305.
14. Park,H.W. and Guan,K.L. (2013) Regulation of the hippo pathway and implications for anticancer drug development. *Trends Pharm. Sci.*, **34**, 581–589.
15. Liu,R., Lee,J., Kim,B.S., Wang,Q., Buxton,S.K., Balasubramanyam,N., Kim,J.J., Dong,J., Zhang,A., Li,S. *et al.* (2017) Tead1 is required for maintaining adult cardiomyocyte function, and its loss results in lethal dilated cardiomyopathy. *JCI Insight.*, **2**, e93343.
16. Liu,F., Wang,X., Hu,G., Wang,Y. and Zhou,J. (2014) The transcription factor TEAD1 represses smooth muscle-specific gene expression by abolishing myocardin function. *J. Biol. Chem.*, **289**, 3308–3316.
17. Rahier,J, Guiot,Y, Goebbels,RM, Sempoux,C and Henquin,JC (2008) Pancreatic beta-cell mass in european subjects with type 2 diabetes. *Diabetes Obes. Metab.*, **10**, 32–42.
18. Pullen,T.J., Khan,A.M., Barton,G., Butcher,S.A., Sun,G. and Rutter,G.A. (2010) Identification of genes selectively disallowed in the pancreatic islet. *Islets*, **2**, 89–95.
19. Rosado-Olivieri,E.A., Anderson,K., Kenty,J.H. and Melton,D.A. (2019) YAP inhibition enhances the differentiation of functional stem cell-derived insulin-producing β cells. *Nat. Commun.*, **10**, 1464.
20. George,NM, Day,CE, Boerner,BP, Johnson,RL and Sarvetnick,NE. (2012) Hippo signaling regulates pancreas development through inactivation of yap. *Mol. Cell. Biol.*, **32**, 5116–5128.
21. Gao,T., Zhou,D., Yang,C., Singh,T., Penzo-Méndez,A., Maddipati,R., Tzatsos,A., Bardeesy,N., Avruch,J. and Stanger,B.Z. (2013) Hippo signaling regulates differentiation and maintenance in the exocrine pancreas. *Gastroenterology*, **144**, 1543–1553.
22. Lee,J., Liu,R., Kim,B.S., Zhang,Y., Li,F., Jagannathan,R., Yang,P., Negi,V., Perez-Garcia,E.M., Saha,P.K. *et al.*Tead1 reciprocally regulates adult β-cell proliferation and function. bioRxiv doi: https://doi.org/10.1101/2020.03.05.979450, preprint: not peer reviewed.
23. Tomczak,K, Czerwinska,P and Wiznerowicz,M (2015) The cancer genome atlas (TCGA): an immeasurable source of knowledge. *Contemp Oncol (Pozn).*, **19**, A68–A77.
24. Jiang,X., Cao,Y., Li,F., Su,Y., Li,Y., Peng,Y., Cheng,Y., Zhang,C., Wang,W. and Ning,G. (2014) Targeting β-catenin signaling for therapeutic intervention in MEN1-deficient pancreatic neuroendocrine tumours. *Nat. Commun.*, **5**, 5809.
25. Phelps,E.A., Cianciaruso,C., Santo-Domingo,J., Pasquier,M., Galliverti,G., Piemonti,L., Berishvili,E., Burri,O., Wiederkehr,A., Jeffrey,A. *et al.* (2017) Advances in pancreatic islet monolayer culture on glass surfaces enable super-resolution microscopy and insights into beta cell ciliogenesis and proliferation. *Sci. Rep.*, **7**, 45961.
26. NG,K. and Gumbiner,BM. (2015) Adhesion to fibronectin regulates hippo signaling via the FAK-Src-PI3K pathway. *J. Cell Biol.*, **210**, 503–515.
27. Oki,S., Ohta,T., Shioi,G., Hatanaka,H., Ogasawara,O., Okuda,Y., Kawaji,H., Nakaki,R. and Sese,J.*Chikara Meno*. (2018) ChIP-Atlas: a data-mining suite powered by full integration of public chip-seq data. *EMBO Rep.*, **19**, e46255.
28. Cebola,I., Rodríguez-Seguí,S.A., Cho,C.H., Bessa,J., Rovira,M., Luengo,M., Chhatriwala,M., Berry,A., Ponsa-Cobas,J., Maestro,M.A. *et al.* (2015) TEAD and YAP regulate the enhancer network of human embryonic pancreatic progenitors. *Nat. Cell Biol.*, **17**, 615–626.
29. Bonner-Weir,S., Aguayo-Mazzucato,C. and Weir,G.C. (2016) Dynamic development of the pancreas from birth to adulthood. *Ups. J. Med. Sci.*, **121**, 155–158.
30. Maeder,M.L., Linder,S.J., Cascio,V.M., Fu,Y., Ho,Q.H. and Joung,J. (2013) CRISPR RNA-guided activation of endogenous human genes. *Nat. Methods*, **10**, 977–979.
31. Cabantous,S., Nguyen,H., Pedelacq,J., Koraïchi,F., Chaudhary,A., Ganguly,K., Lockard,M.A., Favre,G., Terwilliger,T.C. and Waldo,G.S. (2013) A new protein-protein interaction sensor based on tripartite Split-GFP association. *Sci. Rep.*, **3**, 2854.
32. Hoa,L., Kulaberoglu,Y., Gundogdu,R., Cook,D., Mavis,M., Gomez,M., Gomez,V. and Hergovich,A. (2016) The characterisation of LATS2 kinase regulation in Hippo-YAP signaling. *Cell Signal*, **28**, 488–497.
33. Hermann,A., Wu,G., Nedvetsky,P.I., Brücher,V.C., Egbring,C., Bonse,J., Höffken,V., Wennmann,D.O., Marks,M., Krahn,M.P. *et al.* (2021) The hippo pathway component wwc2 is a key regulator of embryonic development and angiogenesis in mice. *Cell Death Dis.*, **12**, 117.
34. Zhao,B, Li,L, Lu,Q, Wang,LH, Liu,CY, Lei,Q and Guan,KL. (2011) Angiomotin is a novel hippo pathway component that inhibits YAP oncoprotein. *Genes Dev.*, **25**, 51–63.
35. Keyvani Chahi,A., Martin,C.E. and Jones,N. (2016) Nephrin suppresses hippo signaling through the adaptor proteins nck and WTIP. *J. Biol. Chem.*, **291**, 12799–12808.
36. Maltais,A and Labelle,Y (2000) Structure and expression of the mouse gene encoding the orphan nuclear receptor TEC. *DNA Cell Biol.*, **19**, 121–130.
37. Nagaoka,M., Yashiro,T., Uchida,Y., Ando,T., Hara,M., Arai,H., Ogawa,H., Okumura,K., Kasakura,K. and Nishiyama,C. (2017) The orphan nuclear receptor NR4A3 is involved in the function of dendritic cells. *J. Immunol.*, **199**, 2958–2967.
38. Tessem,JS, Moss,LG, Chao,LC, Arlotto,M, Lu,D, Jensen,MV, Stephens,SB, Tontonoz,P, Hohmeier,HE and Newgard,CB. (2014) Nkx6.1 regulates islet beta-cell proliferation via Nr4a1 and Nr4a3 nuclear receptors. *Proc. Natl. Acad. Sci. U.S.A.*, **111**, 5242–5247.
39. Close,AF, Dadheech,N, Villela,BS, Rouillard,C and Buteau,J. (2019) The orphan nuclear receptor nor1/nr4a3 is a negative regulator of beta-cell mass. *J. Biol. Chem.*, **294**, 4889–4897.
40. George,N.M., Boerner,B.P., Mir,S.U., Guinn,Z. and Sarvetnick,N.E. (2015) Exploiting expression of hippo effector, yap, for expansion of functional islet mass. *Mol. Endocrinol.*, **29**, 1594–1607.
41. Wang,C., Zhu,X., Feng,W., Yu,Y., Jeong,K., Guo,W., Lu,Y. and Mills,G.B. (2015) Verteporfin inhibits YAP function through up-regulating 14-3-3σ sequestering YAP in the cytoplasm. *Am. J. Cancer Res.*, **6**, 27–37.
42. Crawford,L.A., Guney,M.A., Oh,.A., Andrea Deyoung,R, Valenzuela,D.M., Murphy,A.J., Yancopoulos,G.D., Lyons,K.M., Brigstock,D.R., Economides,A. *et al.* (2009) Connective tissue growth factor (CTGF) inactivation leads to defects in islet cell lineage allocation and beta-cell proliferation during embryogenesis. *Mol. Endocrinol.*, **23**, 324–336.
43. Calses,P.C., Crawford,J.J., Lill,J.R. and Dey,A. (2019) Hippo pathway in cancer: aberrant regulation and therapeutic opportunities. *Trends Cancer*, **5**, 297–307.
44. Gill,M.K., Christova,T., Zhang,Y.Y., Gregorieff,A., Zhang,L., Narimatsu,M., Song,S., Xiong,S., Couzens,A.L., Tong,J. *et al.* (2018)

A feed forward loop enforces YAP/TAZ signaling during tumorigenesis. *Nat. Commun.*, **9**, 3510.
45. Lu,T., Li,Y., Lu,W., Spitters,T., Fang,X., Wang,J., Cai,S., Gao,J., Zhou,Y., Duan,Z. *et al.* (2021) Discovery of a subtype-selective, covalent inhibitor against palmitoylation pocket of TEAD3. *Acta Pharm Sin. B.*, **11**, 3206–3219.
46. He,C, Lv,X, Huang,C, Hua,G, Ma,B, Chen,X, Angeletti,PC, Dong,J, Zhou,J, Wang,Z *et al.* (2019) YAP1-LATS2 feedback loop dictates senescent or malignant cell fate to maintain tissue homeostasis. *EMBO Rep.*, **20**, e44948.
47. Tsika,R.W., Ma,L., Kehat,I., Schramm,C., Simmer,G., Morgan,B., Fine,D.M., Hanft,L.M., McDonald,K.S., Molkentin,J.D. *et al.* (2010) TEAD-1 overexpression in the mouse heart promotes an age-dependent heart dysfunction. *J. Biol. Chem.*, **285**, 13721–13735.
48. Huh,H.D., Kim,D.H., Jeong,H. and Park,H.W. (2019) Regulation of TEAD transcription factors in cancer biology. *Cells*, **8**, 600.
49. Joshi,S., Davidson,G., Le Gras,S., Watanabe,S., Braun,T., Mengus,G. and Davidson,I. (2017) TEAD transcription factors are required for normal primary myoblast differentiation in vitro and muscle regeneration in vivo. *PLos Genet.*, **13**, e1006600.
50. Anbanandam,A., Albarado,D.C., Nguyen,C.T., Halder,G., Gao,X. and Veeraraghavan,S. (2006) Insights into transcription enhancer factor 1 (TEF-1) activity from the solution structure of the TEA domain. *Proc. Natl. Acad. Sci. U.S.A.*, **103**, 17225–17230.
51. Lakhin,A.V., Tarantul,V.Z. and Gening,L.V. (2013) Aptamers: problems, solutions and prospects. *Acta Naturae*, **5**, 34–43